

A Hybrid NOMA-OMA Scheme for Inter-plane Intersatellite Communications in Massive LEO Constellations

Donatella Darsena, *Senior Member, IEEE*, Giacinto Gelli, *Senior Member, IEEE*,
Ivan Iudice, and Francesco Verde, *Senior Member, IEEE*

Abstract

Communication between satellites in low-Earth orbit (LEO) constellations takes place through inter-satellite links (ISLs). Unlike intra-plane ISLs, which interconnect satellites belonging to the same orbital plane with fixed relative distance, inter-plane ISLs experience significant Doppler frequency shifts, since satellites belonging to different orbital planes exhibit time-varying relative distance (required, e.g., to minimize the risk of physical collisions between satellites). In this paper, we consider the problem of connecting multiple satellites, belonging a massive LEO Walker Delta constellation, to a receiving satellite, referred to as the sink. Specifically, we consider a hybrid multiple access scheme, which employs a combination of non-orthogonal multiple access (NOMA), where ISLs share the same time-frequency resource blocks, and orthogonal multiple access (OMA), where ISLs employs orthogonal resource blocks. To this aim, the set of satellites transmitting towards the sink is divided into groups, where NOMA is employed within each group, whereas OMA is used to separate different groups. Such a scheme subsumes as special cases both pure-OMA and pure-NOMA. Our study highlights that similar Doppler frequency shifts have a large impact on the individual rates of the satellites in a pure-NOMA scheme, thus reducing the network fairness of this technique. Motivated by such a fact, we develop design strategies of the proposed hybrid NOMA-OMA scheme, which exploit inter-plane Doppler frequency diversity to enhance fairness among the satellites, while ensuring a significantly higher sum-rate capacity compared to the pure-OMA technique. Numerical results corroborate our theoretical analysis, by demonstrating both the fairness enhancement of the proposed techniques over the pure-NOMA scheme, as well as their capacity improvement over the pure-OMA one.

Index Terms

Capacity, Doppler frequency diversity, fairness, Low-Earth orbit (LEO) constellations, non-orthogonal multiple access (NOMA), orthogonal multiple access (OMA), resource allocation, superposition coding, successive interference cancellation (SIC).

I. INTRODUCTION

There is an upsurge of interest, both in the industrial and academic community, towards *low-Earth orbit* (LEO) satellite constellations, whose satellites are deployed between 400 and 2000 km over the Earth surface. Compared to higher orbits, LEO constellations offer better

D. Darsena, G. Gelli, and F. Verde are with the Department of Electrical Engineering and Information Technology, University Federico II, Naples I-80125, Italy [e-mail: (darsena, gelli, f.verde)@unina.it]. I. Iudice is with the Reliability & Security Department, Italian Aerospace Research Centre (CIRA), Capua I-81043, Italy (e-mail: i.iudice@cira.it). D. Darsena, G. Gelli, and F. Verde are also with National Inter-University Consortium for Telecommunications (CNIT).

The research activities presented in this paper fall within the fields of interest of the IEEE AESS technical panel on Glue Technologies for Space Systems.

coverage and reduced propagation delays. Such advantages have spurred also standardization activities, e.g., within 3GPP, to integrate LEO satellite networks in 5G and beyond-5G networks [1], [2]. In addition to national/international public institutions, an increasing number of private companies (e.g., SpaceX, OneWeb, Amazon, and Google) have planned and started to deploy LEO constellations composed by thousands of satellites – so called *megaconstellations* – with the aim of providing global services, such as broadband Internet access and mobile telephony, as well as to support Internet-of-Remote-Things (IoRT) applications [3]. In such megaconstellations, satellites are typically organized in groups, each one following the same orbital trajectory, which lies in a plane called *orbital plane* (OP). The angle between the OP and the equatorial plane is called *inclination*, ranging from 0° (equatorial orbits) to nearly 90° (polar orbits). For instance, the Starlink megaconstellation envisioned by SpaceX is expected to be comprised by approximately 12000 LEO and very LEO (i.e., under 400 km) satellites, to be deployed in two phases. In phase I, SpaceX is deploying a LEO constellation of 1584 satellites, arranged in 22 orbital planes (OPs), with 72 satellites per OP, at an altitude of 550 km and an inclination of 53° .

In next-generation LEO satellite networks, it is commonly recognized [4] that *intersatellite links* (ISLs) will play an important role to satisfy challenging performance requirements, in terms of connectivity, coverage, capacity, and latency. Traditional ISL designs for geostationary orbit (GEO) systems must be rethought, to be adapted to the dynamic features of LEO satellite network, which are characterized by relative low-power transmission capabilities and high mobility. Since satellites in the same OP are at the same altitude and move with the same velocity, their relative position does not change over time and, hence, *intraorbital plane* (intra-OP) ISLs are relatively easy to be established and managed. Instead, *interorbital plane* (inter-OP) ISLs are more difficult to deal with, since the satellites move with different speeds and hence experiment high Doppler frequency shifts and demand high challenges to acquisition, tracking, and pointing (ATP) systems.

To avoid interference between ISLs caused by the sharing of wireless resources by multiple communicating satellites [5], state-of-the-art satellite communications mainly adopt *orthogonal multiple access* (OMA) schemes, such as frequency division multiple access (FDMA), time-division multiple access (TDMA), code-division multiple access (CDMA), orthogonal frequency-division multiple access (OFDMA), or combinations thereof. In recent years, *non-orthogonal multiple access* (NOMA) has been recognized [6] as a promising technique for terrestrial networks, due to its superior spectral efficiency with respect to OMA schemes. Indeed, in NOMA, multiple users are allowed to share the same time-frequency resource (or pool of resources), through power-domain or code-domain multiplexing. The superimposed signals can be separated at the receiver by

using successive interference cancellation (SIC). At the cost of an increased receiver complexity, NOMA techniques offer not only improved spectral efficiency, but also fairness in some cases [7].

The focus of this paper is on design of multiple access strategies for LEO megaconstellations, which leverages the different Doppler profiles (so called *Doppler diversity*) of the satellites.

A. Related work and open research

Some works have considered NOMA for satellite networks (see [8] and references therein), but are mainly limited to air-to-ground (downlink) or ground-to-air (uplink) communications. A power-domain NOMA scheme for the downlink of an integrated satellite-terrestrial network was considered in [3], targeted at IoT applications. With particular reference to LEO constellations, the performance analysis of downlink NOMA is carried out in [9], in terms of ergodic capacity, outage probability, and mutual information, by considering the case of two ground users in one spot beam. In [10], the sum-rate capacity maximization problem was considered for a LEO constellation employing massive MIMO in conjunction with NOMA. In [11], a NOMA scheme has been introduced in uplink, in the context of a multi-layer satellite networks, composed by GEO and LEO satellites. The works [3], [9]–[11] do not consider intersatellite (IS) communication at all.

The problem of IS communication has been studied in [12], where communications between two satellite groups are established with the help of a relay satellite and applying NOMA schemes for both downlink and uplink. NOMA schemes for a dual-layer LEO megaconstellation are studied in [13], aimed at allowing the coexistence of services with different requirements. However, in [12], [13], Doppler frequency shifts are regarded as a cause of performance degradation rather than as a source of diversity.

The design of ISLs for dense LEO constellations has been considered in [5], where the establishment of inter-OP ISLs is casted as a weighted dynamic matching problem and solved by performing sum-rate capacity maximization. However, this research considers an OMA scheme and, moreover, marks as *non-feasible* those links characterized by high Doppler frequency shift values. Another work in this area is [14], which deals with the problem of designing inter-OP ISLs, based on reinforcement learning, by discarding links affected by non-negligible Doppler effects.

Henceforth, an open research issue consists of designing multiple access schemes aimed at *exploiting* the Doppler profiles of satellites, rather than *counteracting* the adverse effects of Doppler frequency shifts as commonly done in previous works.

B. Contributions

The contributions of this article are summarized as follows.

- 1) We provide an accurate characterization of the L ISLs that allow multiple satellites of a LEO Walker Delta constellation to effectively communicate with a receiving satellite, referred to as the *sink*. In particular, we unveil that the satellites with feasible ISLs towards the sink belong not only to the same OP of the sink (intra-OP), but also to adjacent and crossing OPs (inter-OP), exhibiting thus significant Doppler frequency shifts.
- 2) We show that the Doppler frequency shifts characterizing inter-OP ISLs have a significant impact on the individual rates of the satellites that access the channel in a non-orthogonal manner with minimum mean-squared error (MMSE)-plus-SIC receiver at the sink, named as *pure-NOMA*, which is optimal for achieving the capacity region of the considered system.
- 3) We develop design procedures of a *hybrid NOMA-OMA* scheme, where the L satellites with *feasible* ISLs towards the sink are partitioned in groups: namely, those belonging to the same group implement NOMA, while the ones belonging to different groups employ OMA. Pure-NOMA and pure-OMA techniques are special cases of such a scheme obtained by setting the number of groups equal to 1 and L , respectively. The objective of the proposed designs is to exploit the differences in Doppler frequency profiles of the superimposed satellite transmissions in order to improve system fairness, by ensuring at the same time a significant performance gain in terms of sum-rate capacity compared to the pure-OMA technique.
- 4) The performance of the considered multiple access schemes is validated numerically. It is demonstrated that exploiting of the inter-plane Doppler frequency diversity is instrumental in achieving a good trade-off between sum-rate capacity and fairness among the satellites.

This article is organized as follows. The mathematical model of the considered system and the characterization of ISLs feasibility are reported in Section II. The MMSE-SIC receiving structure at the sink is described in Section III. A comparative performance study of the pure-OMA, pure-NOMA, and hybrid NOMA-OMA schemes is carried out in Section IV, with particular emphasis on the impact of the frequency Doppler shifts. Design procedures of the proposed hybrid NOMA-OMA scheme are developed in Section V, and related numerical results are reported in Section VI. Finally, the main results obtained in this article are summarized and discussed in Section VII.

II. SYSTEM MODEL

Let us consider a general LEO Walker Delta constellation, composed of K satellites, uniformly-distributed and equally-spaced in P OPs. Each satellite follows a circular orbit around the Earth,

at a given altitude h above the terrestrial surface, having an inclination α with respect to the equatorial plane, and phasing parameter F [15].

Let $N \triangleq K/P$ (assumed to be an integer) denote the number of satellites in each OP. In order to univocally identify every satellite, we use the couple of indices (p, n) indicating the n -th satellite in the p -th orbital plane, for $n \in \{1, 2, \dots, N\}$ and $p \in \{1, 2, \dots, P\}$. We investigate the establishment of ISLs between a number of transmitting satellites,¹ belonging to a group or *swarm*, towards a receiving satellite, referred to as the *sink* in the following. In particular, without loss of generality, we choose the satellite $(1, 1)$ as the communication sink.

A. Conditions ensuring ISL feasibility

Herein, we investigate the problem of assuring a reliable communication link between the satellites of each group and the sink, so called *ISL feasibility*, which is influenced by the following aspects: (i) line-of-sight (LoS) propagation; (ii) satellite antenna radiation pattern; (iii) path loss and receiver sensitivity. To study the first aspect, we introduce the customary Earth-Centered Earth-Fixed (ECEF) right-handed orthogonal coordinate system (or *frame*), with origin at the center of Earth and z axis coincident with the oriented line from South pole to North pole. Assuming the Earth shape to be spherical, with average radius $R = 6378$ km, the position of the satellite (p, n) , deployed at altitude h above Earth, is defined in the ECEF frame by the spherical coordinate triple $(R + h, \theta_{p,n}, \varphi_{p,n})$, where $\theta_{p,n} \in [0, \pi]$ denotes the polar angle (or *colatitude*) and $\varphi_{p,n} \in [0, 2\pi]$ denotes the azimuthal angle (or *longitude*). Therefore, the distance $d_{p,n}$ between the (p, n) -th satellite and the sink can be calculated with elementary geometry as

$$d_{p,n} = (R + h) \{2 [1 - \cos(\theta_{p,n}) \cos(\theta_{1,1}) - \sin(\theta_{p,n}) \sin(\theta_{1,1}) \cos(\varphi_{p,n} - \varphi_{1,1})]\}^{1/2}. \quad (1)$$

The corresponding ISL is in visibility [16] if condition

$$(\mathbf{c1}) : d_{p,n} \leq d_{\text{horiz}} \quad (2)$$

holds, where $d_{\text{horiz}} \triangleq 2[h(h + 2R)]^{1/2}$ is the radio horizon.

Let us consider antenna radiation pattern limitations. Usually, a spacecraft is equipped with intra-plane ISL antennas located at both sides of the roll axis (aligned to the satellite speed vector) and inter-plane ISL antennas along the pitch axis (perpendicular to the orbit plane), as shown in Fig. 1. Hereinafter, we assume that each satellite is equipped with highly-directional

¹ISLs can be implemented with radio-frequency (RF), including those operating in the new Terahertz (THz) band, or optical technologies. Although the models in this paper assume RF technologies, many of the proposed solutions can be readily adapted to the optical case.

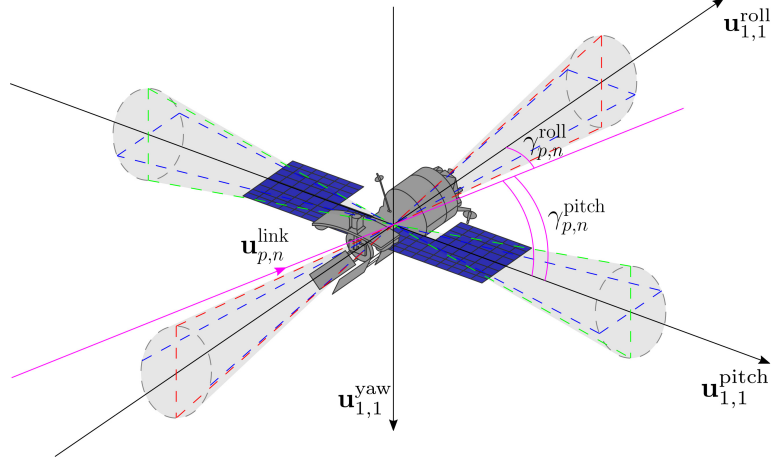


Fig. 1. The ISL antenna beams of the sink.

wideband antennas, with approximately conical beams, whose half-beamwidths are denoted with $\beta_{p,n}$ (assumed to be equal for all the antennas on board each satellite). Under these assumptions, a feasible LoS link between satellite $(p, n) \neq (1, 1)$ and the sink $(1, 1)$ can be established only if the corresponding RF propagation direction falls within the antenna beams. Henceforth, let $\gamma_{p,n}^{\text{pitch}}$ and $\gamma_{p,n}^{\text{roll}}$ denote the angles between $\mathbf{u}_{p,n}^{\text{link}}$, i.e., the direction of propagation of the signal emitted by the (p, n) -th satellite², and the pitch and roll axes of the sink, given respectively by $\mathbf{u}_{1,1}^{\text{pitch}}$ and $\mathbf{u}_{1,1}^{\text{roll}}$ (see Fig. 1), the following condition must hold

$$(\mathbf{c2}) : \{\gamma_{p,n}^{\text{pitch}} \leq \beta_{1,1}\} \cup \{\gamma_{p,n}^{\text{roll}} \leq \beta_{1,1}\} \quad \text{for } (p, n) \neq (1, 1). \quad (3)$$

Finally, we take into account receiver sensitivity and losses due to free-space propagation. Indeed, for LEO satellites, propagation occurs mainly in the *thermosphere*, where the air molecule density is very low, hence loss mechanisms due to molecular absorption and scattering are practically absent [17]. Consequently, we adopt for the path loss the common Friis model [16]

$$P_{p,n}^{\text{rx}} = P_{p,n}^{\text{tx}} G_{p,n}^{\text{tx}} G_{1,1}^{\text{rx}} \left(\frac{\lambda_c}{4\pi d_{p,n}} \right)^2 \quad (4)$$

where $P_{p,n}^{\text{tx}}$ and $P_{p,n}^{\text{rx}}$ are the power transmitted by the (p, n) -th satellite and received at the sink, respectively, $G_{p,n}^{\text{tx}}$ and $G_{1,1}^{\text{rx}}$ represent the antenna gains of the (p, n) -th transmitting satellite and sink, respectively, λ_c is the signal wavelength, and $d_{p,n}$ denotes the distance between transmit and receive antennas. When the wavelength is very small, the *geometric path loss* $(4\pi d_{p,n}/\lambda_c)^2$

²We are assuming that the signal emitted by the (p, n) -th satellite propagates only if the line-of-sight of the sink from the (p, n) -th satellite standpoint falls within the transmitter antenna beam.

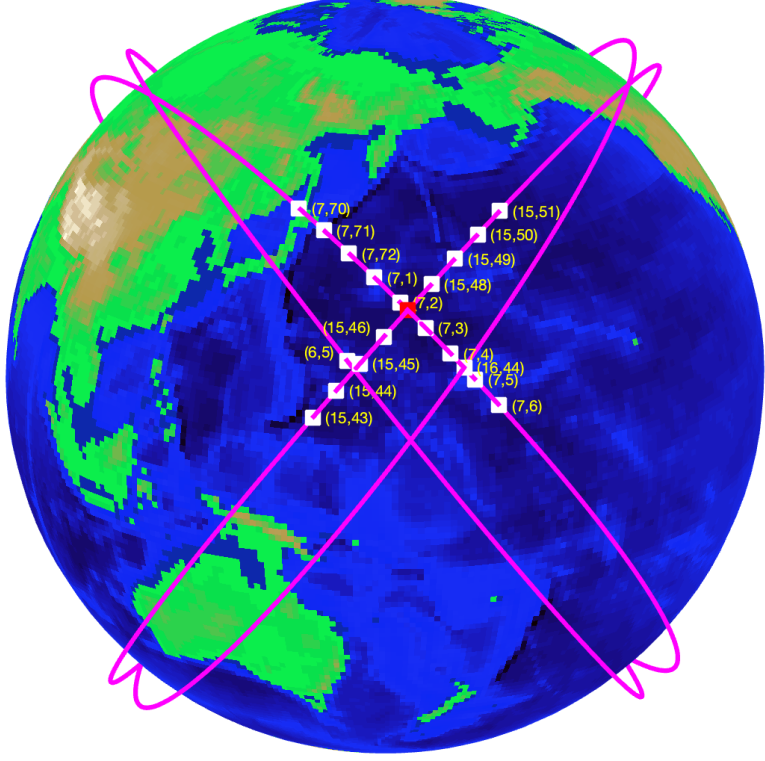


Fig. 2. A pictorial view of all the satellites with feasible ISLs towards the sink represented by the satellite with indices (15, 47) (i.e., the red square in the figure).

is considerable, so highly-directional antennas with high gains are required. Therefore, for the propagation link between the (p, n) -th transmitting satellite and sink, the power $P_{p,n}^{\text{rx}}$ has to fulfill

$$(\mathbf{c3}) : P_{p,n}^{\text{rx}} \geq P_{\text{sens}}^{\text{rx}} \quad (5)$$

where the receiver sensitivity $P_{\text{sens}}^{\text{rx}}$ represents the lowest value of the received power at which the signal can be decoded satisfactorily, i.e., with a given bit-error-rate (BER).

Definition 1 (Feasible ISLs). Only those satellites that satisfy the *three* ISL feasibility requirements **(c1)**, **(c2)**, and **(c3)**, can effectively communicate with the sink. The set \mathcal{C} contains all the couples (p, n) satisfying (2)-(5) and $L \triangleq \text{card}(\mathcal{C}) \leq K$ is the number of feasible ISLs.

As an illustrative example, we consider a LEO Walker Delta constellation composed of $K = 1584$ satellites flying over $P = 22$ OPs at altitude $h = 550$ km. The number of satellites per OP is $N = K/P = 72$, the inclination with respect to the equatorial plane is $\alpha = 53^\circ$, and the phasing parameter is set equal to $F = 17$. Moreover, the period of revolution of the satellites is 91 minutes. With reference to an observation interval of length 0.5 ms, we report in Fig. 2 a pictorial representation of the satellites having feasible ISLs with respect to the sink, corresponding to the

satellite having indices $(15, 47)$. In this example, the signal carrier frequency $f_c = c/\lambda_c$ is 40 GHz, with c denoting the speed of light in the vacuum, the power transmitted by the satellites is $P_{p,n}^{\text{tx}} = 10$ W, the transmit and receive antenna maximum gains are set equal to 23 dB, the receiver sensitivity is $P_{\text{sens}}^{\text{rx}} = -120$ dBm. It is seen that, in the considered observation interval, the number of satellites with feasible ISLs towards the sink³ is $L = 19$, whose indices constituting the set \mathcal{C} are explicitly indicated in Fig. 2.

In the subsequent models, to simplify further developments, it is assumed that a suitable mapping, which transforms each couple $(p, n) \in \mathcal{C}$ into a one-dimensional index $\ell \in \mathcal{L} \triangleq \{1, 2, \dots, L\}$, has been introduced.

B. The proposed multiple-access transmission scheme

We briefly introduce herewith the proposed multiple-access scheme (further details are given in Sections III and IV). For a given value of $G \in \{1, 2, \dots, L\}$, let $\mathbb{P}(\mathcal{L}) = \{\mathcal{L}_k\}_{k=1}^G$ be a partition of \mathcal{L} , i.e., $\cup_{k=1}^G \mathcal{L}_k = \mathcal{L}$ and $\mathcal{L}_k \cap \mathcal{L}_h = \emptyset$ for $k \neq h$, with $\sum_{k=1}^G L_k = L$, where $L_k \triangleq \text{card}(\mathcal{L}_k)$. Our aim is to determine $\mathbb{P}(\mathcal{L})$ such that the satellites that are members of the group \mathcal{L}_k concurrently transmit by employing a NOMA scheme, based on superposition coding (SC) and successive interference cancellation (SIC) at the receiver, whereas the satellites belonging to different groups \mathcal{L}_k and \mathcal{L}_h , with $k \neq h$, transmit by employing an OMA scheme over non-interfering links. It is noteworthy that it is irrelevant for a capacity analysis whether the partitioning is across time or frequency (or both), since the power constraint is on the average across the degrees of freedom (DoF) [18].

We would like to recall attention to two extreme cases: when $G = 1$ and, thus, $L_1 = L$, all the L satellites with feasible links transmit over the same time-frequency resources by using the SC-SIC scheme and, in this case, one has a *pure-NOMA* technique. On the other hand, when $G = L$ and, thus, $L_k = 1$, the sink receives orthogonal signals from the L different satellites and, in this case, the proposed scheme boils down to a *pure-OMA* technique. For the intermediate values of $G \in \{2, 3, \dots, L - 1\}$, the satellites communicate with the sink through a *hybrid NOMA-OMA* transmission scheme.

C. Model of the signal received by the group \mathcal{L}_k

We assume that the partition $\mathbb{P}(\mathcal{L})$ has been determined and, without loss of generality, we focus on NOMA communication within the k -th satellite group $\mathcal{L}_k \triangleq \{\ell_{k,1}, \ell_{k,2}, \dots, \ell_{k,L_k}\}$, for

³It can also be shown that 19 is the maximum number of satellites with feasible ISLs throughout the revolution period of satellites.

$k \in \{1, 2, \dots, G\}$. Moreover, let T be the symbol period, $\{b_{\ell_{k,q}}(h)\} \in \mathbb{C}$ the sequence sent by the $(\ell_{k,q})$ -th satellite in the h -th symbol interval, with $h \in \mathbb{Z}$ and $q \in \{1, 2, \dots, L_k\}$, and $p(t)$ the impulse response of the cascade of the transmit/receive shaping filters. We assume that $p(t) \approx 0 \forall t \notin [0, T]$. Assuming a linear modulation, the baseband signal of the $(\ell_{k,q})$ -th satellite passed through the transmit and receive shaping filters is given by

$$x_{\ell_{k,q}}(t) = \frac{1}{\sqrt{\rho_k}} \sum_{h=-\infty}^{+\infty} b_{\ell_{k,q}}(h) p(t - hT), \quad \text{for } t \in [0, T_0] \quad (6)$$

where T_0 is the length of the observation interval and ρ_k is the fraction of DoF allocated to all the satellites belonging to the group \mathcal{L}_k , with

$$\sum_{k=1}^G \rho_k = 1. \quad (7)$$

The transmitted symbols $\{b_{\ell_{k,q}}(h)\}_{h \in \mathbb{Z}}$ are modeled as mutually independent sequences of zero-mean unit-variance independent and identically distributed (i.i.d.) complex circularly-symmetric random variables. Hereinafter, we assume that the $(\ell_{k,q})$ -th satellite is moving (relative to the sink) at constant *radial* speed $v_{\ell_{k,q}}$ within the observation interval. In this case, the time-varying distance covered by the wavefront transmitted by the satellite $\ell_{k,q}$ and received at the sink is given by $d_{\ell_{k,q}}(t) = d_{\ell_{k,q}}(0) + v_{\ell_{k,q}} t$, for $t \in [0, T_0]$. Under the mild assumption that $|v_{\ell_{k,q}}| T_0 \ll |d_{\ell_{k,q}}(0)|$, the Doppler effect induces a simple carrier frequency shift [19] and, thus, the far-field noise-free signal $r_k(t)$ received by the sink from the k -th satellite group can be expressed as

$$r_k(t) = \sum_{q=1}^{L_k} A_{\ell_{k,q}} e^{j2\pi f_{\ell_{k,q}} t} x_{\ell_{k,q}}(t - \tau_{\ell_{k,q}}) \quad (8)$$

for $t \in [0, T_0]$, where $A_{\ell_{k,q}}$, $f_{\ell_{k,q}}$, and $\tau_{\ell_{k,q}}$ are the complex amplitude, Doppler frequency shift, and delay, respectively, of the link between the $(\ell_{k,q})$ -th satellite and the sink. Model (8) has been derived under the additional assumption that $f_{k,\max} T \ll 1$ [20], where $f_{k,\max} \triangleq \max_{q \in \{1, 2, \dots, L_k\}} |f_{\ell_{k,q}}|$ is the maximum Doppler frequency shift in \mathcal{L}_k . It should be noted that the argument of $A_{\ell_{k,q}}$ accounts for a phase misalignment between the $(\ell_{k,q})$ -th satellite and the sink.

In the following, we will assume that a timing advance (TA) scheme is employed [21], such that the signals transmitted by satellites within the same time interval arrive nearly aligned at the sink. In this case, $\tau_{\ell_{k,q}} \approx \tau_0$ in (8) and timing misalignment interference is avoided. Without loss of generality, we set hereinafter $\tau_0 = 0$ to simplify the forthcoming derivations.

At the sink, to demodulate the symbols received in the interval $[uT, (u+1)T] \subseteq [0, T_0]$ ($u \in \mathbb{Z}$), the signal (8) is sampled with rate $1/T_c \triangleq S/T$ at instants $t_{u,s} \triangleq uT + sT_c$, for

$s \in \{0, 1, \dots, S-1\}$, with $S > 1$ denoting the oversampling factor. Let $r_k^{(s)}[u] \triangleq r_k(t_{u,s})$ be the discrete-time version of (8), for $u \in \{0, 1, \dots, N_0-1\}$, one gets

$$r_k^{(s)}[u] = \sum_{q=1}^{L_k} \frac{A_{\ell_{k,q}}}{\sqrt{\rho_k}} e^{j2\pi S \nu_{\ell_{k,q}} u} e^{j2\pi \nu_{\ell_{k,q}} s} p(s T_c) b_{\ell_{k,q}}[u] \quad (9)$$

with $N_0 \triangleq T_0/T$ (assumed to be an integer for simplicity), $\nu_{\ell_{k,q}} \triangleq f_{\ell_{k,q}} T_c \in [0, 1)$ denoting the *normalized* Doppler frequency shift.

Let $\mathbf{r}_k[u] \triangleq [r_k^{(0)}[u], r_k^{(1)}[u], \dots, r_k^{(S-1)}[u]]^T \in \mathbb{C}^S$, it results that, for $u \in \{0, 1, \dots, N_0-1\}$,

$$\begin{aligned} \mathbf{r}_k[u] &= \sum_{q=1}^{L_k} \frac{A_{\ell_{k,q}}}{\sqrt{\rho_k}} e^{j2\pi S \nu_{\ell_{k,q}} u} \mathbf{P} \mathbf{v}_{\ell_{k,q}} b_{\ell_{k,q}}[u] \\ &= \frac{1}{\sqrt{\rho_k}} \sum_{q=1}^{L_k} \tilde{\mathbf{h}}_{\ell_{k,q}}[u] b_{\ell_{k,q}}[u] \end{aligned} \quad (10)$$

where $\tilde{\mathbf{h}}_{\ell_{k,q}}[u] \triangleq A_{\ell_{k,q}} e^{j2\pi S \nu_{\ell_{k,q}} u} \mathbf{P} \mathbf{v}_{\ell_{k,q}} \in \mathbb{C}^S$ represents the time-varying *composite* channel response of the $(\ell_{k,q})$ -th ISL, with $\mathbf{P} \triangleq \text{diag}[p(0), p(T_c), \dots, p((S-1)T_c)] \in \mathbb{R}^{S \times S}$ and Vandermonde vector $\mathbf{v}_{\ell_{k,q}} \triangleq [1, e^{j2\pi \nu_{\ell_{k,q}}}, \dots, e^{j2\pi \nu_{\ell_{k,q}}(S-1)}]^T \in \mathbb{C}^S$. In the sequel, we assume that the pulse shaping filter $p(t)$ and the sampling period T_c are chosen such that \mathbf{P} is non-singular.

III. SIGNAL DETECTION

In this section, we describe the reception strategy adopted in the proposed NOMA scheme. We assume that the sink is perfectly aware of all channel parameters in (10), i.e., complex amplitudes $A_{\ell_{k,q}}$ and normalized Doppler frequency shifts $\nu_{\ell_{k,q}}$, which can be calculated from the knowledge of the deterministic motion of the satellites by means of simple geometrical arguments. This knowledge is exploited at the sink to perform simultaneous satellite symbol detection, as explained soon after.

The overall signal received by the sink can be written as

$$\mathbf{r}[u] = \sum_{k=1}^G \mathbf{r}_k[u] + \mathbf{w}[u], \quad \text{for } u \in \{0, 1, \dots, N_0-1\} \quad (11)$$

where $\mathbf{w}[u] \triangleq [w^{(0)}[u], w^{(1)}[u], \dots, w^{(S-1)}[u]]^T \in \mathbb{C}^S$, with $w^{(s)}[u] \triangleq w(t_{u,s})$, and $w(t)$ represents the complex envelope of noise, modeled as a white Gaussian-distributed circularly-symmetric complex random process, with power spectral density σ_w^2 , which is statistically independent of $x_{\ell_{k,q}}(t)$, for any $\ell_{k,q} \in \mathcal{L}_k$ and $k \in \{1, 2, \dots, G\}$. At this point, it is convenient to build a more compact vector model. In particular, let us denote with $\mathbf{b}_k[u] \triangleq [b_{\ell_{k,1}}[u], b_{\ell_{k,2}}[u], \dots, b_{\ell_{k,L_k}}[u]]^T \in$

\mathbb{C}^{L_k} the block collecting the symbols transmitted by all satellites in \mathcal{L}_k , one has from (10) that (11) can be rewritten as

$$\mathbf{r}[u] = \sum_{k=1}^K \tilde{\mathbf{H}}_k[u] \mathbf{b}_k[u] + \mathbf{w}[u] \quad (12)$$

for $u \in \{0, 1, \dots, N_0 - 1\}$, where

$$\begin{aligned} \tilde{\mathbf{H}}_k[u] &\triangleq \frac{1}{\sqrt{\rho_k}} \left[\tilde{\mathbf{h}}_{\ell_{k,1}}[u], \tilde{\mathbf{h}}_{\ell_{k,2}}[u], \dots, \tilde{\mathbf{h}}_{\ell_{k,L_k}}[u] \right] \\ &= \frac{1}{\sqrt{\rho_k}} \mathbf{P} \mathbf{V}_k \mathbf{A}_k \mathbf{E}_k[u] \in \mathbb{C}^{S \times L_k} \end{aligned} \quad (13)$$

with $\mathbf{V}_k \triangleq [\mathbf{v}_{\ell_{k,1}}, \mathbf{v}_{\ell_{k,2}}, \dots, \mathbf{v}_{\ell_{k,L_k}}] \in \mathbb{C}^{S \times L_k}$ being a Vandermonde matrix, whose rank properties will be discussed soon after in Subsection III-D, whereas the diagonal matrices

$$\begin{aligned} \mathbf{A}_k &\triangleq \text{diag}[A_{\ell_{k,1}}, A_{\ell_{k,2}}, \dots, A_{\ell_{k,L_k}}] \in \mathbb{C}^{L_k \times L_k} \\ \mathbf{E}_k[u] &\triangleq \text{diag}[e^{j2\pi S\nu_{\ell_{k,1}} u}, e^{j2\pi S\nu_{\ell_{k,2}} u}, \dots, e^{j2\pi S\nu_{\ell_{k,L_k}} u}] \in \mathbb{C}^{L_k \times L_k} \end{aligned} \quad (14)$$

are non-singular by construction.

We recall that the satellites belonging to different groups \mathcal{L}_k and \mathcal{L}_h , with $k \neq h$, transmit over point-to-point orthogonal links, which have been assigned at a system level by means of a deterministic *channel mapping* procedure. Consequently, the contribution $\mathbf{r}_k[u]$ of the k -th group can be perfectly recovered from (11) through a *channel demapping* operation, thus obtaining

$$\bar{\mathbf{r}}_k[u] \triangleq \mathbf{r}_k[u] + \mathbf{w}_k[u] = \tilde{\mathbf{H}}_k[u] \mathbf{b}_k[u] + \mathbf{w}_k[u] \quad (15)$$

for $u \in \{0, 1, \dots, N_0 - 1\}$, where $\mathbf{w}_k[u]$ is noise after the channel demapping algorithm, which is a circularly-symmetric zero-mean complex Gaussian random vector with covariance matrix $\sigma_w^2 \mathbf{I}_S$.

For each symbol period and satellite group, the detection algorithm consists of an iterative procedure with L_k iterations, which sequentially decodes each entry of $\mathbf{b}_k[u]$, by repeating the following three steps per each iteration: (i) MMSE filtering; (ii) maximum signal-to-interference-plus-noise ratio (SINR) ISL selection; (iii) interference cancellation (SIC).

In Subsections III-A, III-B and III-C, since we focus on the u -th symbol interval and k -th group \mathcal{L}_k , we omit the dependence on both u and k for notational convenience (we maintain the subscript k only for the cardinality L_k).

A. MMSE filtering

Let $\bar{\mathbf{r}}^{(m)} \in \mathbb{C}^S$ denote the input vector of the MMSE filter at the m -th iteration, for $m \in \{0, 1, \dots, L_k - 1\}$, where $\bar{\mathbf{r}}^{(0)} \equiv \bar{\mathbf{r}}$ is given by (15). As a first step, the receiver performs MMSE filtering of $\bar{\mathbf{r}}^{(m)}$ as follows

$$\mathbf{z}^{(m)} \triangleq [z_1^{(m)}, z_2^{(m)}, \dots, z_{L_k-m}^{(m)}]^T = \tilde{\mathbf{F}}^{(m)} \bar{\mathbf{r}}^{(m)} \quad (16)$$

which represents a soft estimate of $\mathbf{b}^{(m)} \in \mathbb{C}^{L_k-m}$, with $\mathbf{b}^{(0)} \equiv \mathbf{b}$, and $\widetilde{\mathbf{F}}^{(m)} \in \mathbb{C}^{(L_k-m) \times S}$ is the solution of the MMSE problem $\min_{\widetilde{\mathbf{F}}^{(m)}} \mathbb{E}[\|\widetilde{\mathbf{F}}^{(m)} \bar{\mathbf{r}}^{(m)} - \mathbf{b}^{(m)}\|^2]$, whose solution is given by

$$\widetilde{\mathbf{F}}^{(m)} = \{\widetilde{\mathbf{H}}^{(m)}\}^H \left[\widetilde{\mathbf{H}}^{(m)} \{\widetilde{\mathbf{H}}^{(m)}\}^H + \sigma_w^2 \mathbf{I}_S \right]^{-1} \quad (17)$$

where $\widetilde{\mathbf{H}}^{(m)} \in \mathbb{C}^{S \times (L_k-m)}$, with $\widetilde{\mathbf{H}}^{(0)} \equiv \widetilde{\mathbf{H}}$. The quantities $\bar{\mathbf{r}}^{(m)}$, $\widetilde{\mathbf{H}}^{(m)}$, and $\mathbf{b}^{(m)}$ iteratively depend on $\bar{\mathbf{r}}^{(m-1)}$, $\widetilde{\mathbf{H}}^{(m-1)}$, and $\mathbf{b}^{(m-1)}$, respectively, as detailed in Subsection III-C.

B. Maximum SINR ISL selection

The maximum SINR (max-SINR) ISL selection algorithm is employed to identify, at each iteration, the “best” ISL, i.e., the entry of the vector $\mathbf{z}^{(m)}$ that exhibits the highest SINR at the output of the MMSE filter. To this aim, at the m -th iteration, the SINR on the ℓ -th entry of $\mathbf{z}^{(m)}$ is given [22] by

$$\text{SINR}_{\ell}^{(m)} = \frac{1}{\sigma_w^2 \left[\left(\sigma_w^2 \mathbf{I}_{L_k-m} + \{\widetilde{\mathbf{H}}^{(m)}\}^H \widetilde{\mathbf{H}}^{(m)} \right)^{-1} \right]_{\ell\ell}} - 1 \quad (18)$$

with $\ell \in \{1, 2, \dots, L_k - m\}$. Hence, at iteration m , we seek the index $\ell_{\max}^{(m)}$ that solves

$$\ell_{\max}^{(m)} = \arg \max_{\ell \in \{1, 2, \dots, L_k - m\}} \text{SINR}_{\ell}^{(m)} \quad (19)$$

and, thus, we get the hard estimate $\widehat{b}_{\ell_{\max}^{(m)}} \triangleq \mathcal{Q}[z_{\ell_{\max}^{(m)}}^{(m)}]$ of $b_{\ell_{\max}^{(m)}}$, where $\mathcal{Q}[\cdot]$ is the minimum-distance decision metric, which depends on the constellation alphabet.

C. Successive interference cancellation (SIC)

The final step of the iterative decoding algorithm consists of cancelling out, at each iteration, the contribution of $\widehat{b}_{\ell_{\max}^{(m)}}$ to the remaining symbols, as

$$\bar{\mathbf{r}}^{(m+1)} = \bar{\mathbf{r}}^{(m)} - \widehat{b}_{\ell_{\max}^{(m)}} \widetilde{\mathbf{h}}_{\ell_{\max}^{(m)}}^{(m)} \quad (20)$$

where $\widetilde{\mathbf{h}}_{\ell_{\max}^{(m)}}^{(m)}$ is the $[\ell_{\max}^{(m)}]$ -th column of $\widetilde{\mathbf{H}}^{(m)}$. Under the simplifying assumption that $\widehat{b}_{\ell_{\max}^{(m)}} \equiv b_{\ell_{\max}^{(m)}}$ (correct decision), the received vector at the $(m+1)$ -th iteration becomes

$$\bar{\mathbf{r}}^{(m+1)} = \widetilde{\mathbf{H}}^{(m+1)} \mathbf{b}^{(m+1)} + \mathbf{w} \quad (21)$$

where the matrix $\widetilde{\mathbf{H}}^{(m+1)}$ is obtained from $\widetilde{\mathbf{H}}^{(m)}$ by removing its $[\ell_{\max}^{(m)}]$ -th column and, similarly, the vector $\mathbf{b}^{(m+1)}$ is obtained from $\mathbf{b}^{(m)}$ by removing its $[\ell_{\max}^{(m)}]$ -th entry.

D. Remarks

The assumption of correct decisions is often invoked when a theoretical capacity analysis is of concern, but of course errors may be made during the SIC process: if one satellite is decoded incorrectly, all subsequent satellites in the same group are affected (so-called *error propagation* phenomenon). If all the satellites are coded with the same target error probability assuming error-free SIC, the effect of error propagation degrades the error probability by a factor of at most the number of satellites L_k [18]. This fact drives one to choose L_k reasonably small such that error propagation effects can be compensated by slightly increasing the coding block length.

As a second remark, we underline that the sum rate of the L_k satellites belonging to the k -th group \mathcal{L}_k is independent of the satellite ordering and achieves the boundary of the multiple-access channel (MAC) capacity region (see Section IV for details). However, the individual rates are affected by the satellite ordering: indeed, satellites decoded at a later stage of the SIC process can benefit from increased throughput. The maximum-SINR ordering described in Subsection III-B guarantees that satellites with better channel conditions are decoded earlier, thus allowing subsequently-decoded weaker satellites to get the best possible rate. Such a sharing strategy ensures *max-min fairness* [23].

A third remark is in order regarding the rank property of $\tilde{\mathbf{H}}_k[u]$ given by (13). Since the diagonal matrices \mathbf{P} , \mathbf{A}_k , and $\mathbf{E}_k[u]$ are non-singular, one has $\text{rank}(\tilde{\mathbf{H}}_k[u]) = \text{rank}(\mathbf{V}_k)$. Relying on the properties of Vandermonde vectors [24], one gets $\text{rank}(\mathbf{V}_k) = \min(S, L_k)$, provided that

$$(\mathbf{c4}) : \nu_{\ell_{k,1}} \neq \nu_{\ell_{k,2}} \neq \dots \neq \nu_{\ell_{k,L_k}}. \quad (22)$$

Condition **(c4)** states that the Doppler frequency shifts of the satellites belonging to the k -th group \mathcal{L}_k have to be (significantly) different from each other in order to obtain a (well-conditioned) full-rank channel matrix. It is worth noticing that not all satellites with feasible ISLs towards the sink (see Definition 1) have different Doppler frequency shifts. To highlight such a fact, we have reported in Table I the Doppler frequency shifts of the $L = 19$ satellites of Fig. 2 (see also Subsection II-A) with feasible ISLs towards the sink (15, 47) in the observation interval of duration $T_0 = 0.5$ ms (corresponding to the transmission of $N_0 = 2000$ symbols at the rate of $1/T = 4$ Mbaud). It is seen from Table I that all the satellites belonging to the same OP of the sink (i.e., those with $p = 15$) essentially exhibit the same Doppler frequency shift, which is very close to zero. However, the satellites that do not belong to the 15-th OP experience high Doppler frequency shifts, especially those flying over the crossing OP 7. As we will show in Section IV,

TABLE I
DOPPLER FREQUENCY SHIFTS OF THE SATELLITES WITH FEASIBLE ISLs TOWARDS THE SINK (15, 47).

Two-dimensional index	One-dimensional index	Doppler frequency shift (Hz)
(6, 5)	1	1.082×10^6
(7, 1)	2	-1.124×10^6
(7, 2)	3	-1.138×10^6
(7, 3)	4	1.113×10^6
(7, 4)	5	1.115×10^6
(7, 5)	6	1.112×10^6
(7, 6)	7	1.106×10^6
(7, 70)	8	-1.103×10^6
(7, 71)	9	-1.111×10^6
(7, 72)	10	-1.118×10^6
(15, 43)	11	3.604×10^{-12}
(15, 44)	12	2.891×10^{-12}
(15, 45)	13	2.591×10^{-12}
(15, 46)	14	1.693×10^{-12}
(15, 48)	15	2.272×10^{-12}
(15, 49)	16	4.359×10^{-12}
(15, 50)	17	7.439×10^{-12}
(15, 51)	18	1.032×10^{-11}
(16, 44)	19	-1.258×10^5

this behavior has a crucial impact on the condition number of the channel matrix $\tilde{\mathbf{H}}_k[u]$ and, thus, on the design of the groups.

A final remark pertains the computational complexity of the proposed time-varying detection algorithm, which is mainly dominated by matrix inversions in (17) and (18), both involving $\mathcal{O}(S^3)$ flops to be repeated for each value of u and m . However, through straightforward manipulations, omitted here for brevity, it can be proven that $\tilde{\mathbf{F}}_k^{(m)}[u]$ can be implemented as the cascade of a time-invariant MMSE filter followed by a time-varying Doppler frequency shift compensation stage, i.e., $\tilde{\mathbf{F}}_k^{(m)}[u] = \{\mathbf{E}_k^{(m)}[u]\}^* \mathbf{F}_k$, where

$$\mathbf{F}_k \triangleq \mathbf{H}_k^H (\mathbf{H}_k \mathbf{H}_k^H + \sigma_w^2 \mathbf{I}_S)^{-1} \in \mathbb{C}^{L_k \times S} \quad (23)$$

with $\mathbf{H}_k \triangleq \mathbf{P} \mathbf{V}_k \mathbf{A}_k / \sqrt{\rho_k} \in \mathbb{C}^{S \times L_k}$ and the diagonal matrix $\mathbf{E}_k^{(m)}[u] \in \mathbb{C}^{L_k \times L_k-m}$ derived from $\mathbf{E}_k^{(m-1)}[u]$ by removing its $[j_{\max}^{(m-1)}]$ -th column, with $\mathbf{E}_k^{(0)}[u] = \mathbf{E}_k[u]$. Such a decomposition entails a reduction of the computational load in evaluating (17), since matrix inversion can be performed only when the iterative algorithm starts and the only time-varying operation boils down to a

multiplication by the diagonal matrix $\{\mathbf{E}_k^{(m)}[u]\}^*$, which is performed at each iteration. As regards SINR calculation in (18), it can be proven that (18) turns out to be time invariant and, moreover, matrix inversion can be done once, i.e., at the start of the iterative algorithm.

IV. SUM-RATE CAPACITY ANALYSIS

Assuming that the satellites encode the information using an i.i.d. Gaussian code, recalled that (18) is time-invariant, the sum rate of the k -th group \mathcal{L}_k is given by

$$\mathcal{R}_k \triangleq \rho_k \sum_{m=0}^{L_k-1} \log_2 \left(1 + \text{SINR}_{k,\ell_{\max}^{(m)}}^{(m)} \right) \quad (\text{in bits/s/Hz}) \quad (24)$$

for $k \in \{1, 2, \dots, G\}$, where $\text{SINR}_{k,\ell}^{(m)}$ has been defined in (18) (with k omitted). After tedious but straightforward algebraic manipulations, it can be verified that

$$\begin{aligned} \mathcal{R}_k &= \rho_k \log_2 \det \left(\mathbf{I}_S + \frac{1}{\sigma_w^2} \tilde{\mathbf{H}}_k[u] \tilde{\mathbf{H}}_k^H[u] \right) \\ &= \rho_k \log_2 \det \left(\mathbf{I}_S + \frac{1}{\sigma_w^2 \rho_k} \mathbf{P} \mathbf{V}_k \mathbf{A}_k \mathbf{A}_k^* \mathbf{V}_k^H \mathbf{P} \right). \end{aligned} \quad (25)$$

We observe that (25) corresponds to the maximum sum rate that can be achieved by the considered system. This confirms the well-known fact that SC at the transmitters and MMSE-SIC at the receiver allow to achieve the boundary of the MAC capacity region [18].

The *sum-rate capacity* of the whole satellite system can be expressed as follows

$$\mathcal{C}_{\text{sum}} \triangleq \sum_{k=1}^G \mathcal{R}_k = \sum_{k=1}^G \rho_k \log_2 \det \left(\mathbf{I}_S + \frac{1}{\sigma_w^2 \rho_k} \mathbf{P} \mathbf{V}_k \mathbf{A}_k \mathbf{A}_k^* \mathbf{V}_k^H \mathbf{P} \right). \quad (26)$$

We provide in the following two subsections a comparative performance analysis in terms of sum-rate capacity of three different multiple access schemes, i.e., pure-NOMA, pure-OMA, and hybrid NOMA-OMA, by unveiling the crucial role played by the Doppler frequency shifts of the satellites that contend for channel resources.

A. Comparison between pure-NOMA and pure-OMA schemes

Eq. (26) subsumes the sum-rate capacity of pure-NOMA and pure-OMA schemes as special cases. Indeed, the sum-rate capacity of the pure-NOMA technique can be obtained from (26) by setting $G = 1$, which implies $L_1 = L$ and $\rho_1 = 1$, i.e., NOMA is implemented among all the L satellites with feasible links, hence yielding

$$\mathcal{C}_{\text{sum}}^{\text{NOMA}} = \log_2 \det \left(\mathbf{I}_S + \frac{1}{\sigma_w^2} \mathbf{P} \mathbf{V} \mathbf{A} \mathbf{A}^* \mathbf{V}^H \mathbf{P} \right) \quad (27)$$

where $\mathbf{V} \triangleq [\mathbf{v}_1, \mathbf{v}_2, \dots, \mathbf{v}_L] \in \mathbb{C}^{S \times L}$ collects all the Vandermonde vectors associated to the L satellites and $\mathbf{A} \triangleq \text{diag}[A_1, A_2, \dots, A_L] \in \mathbb{C}^{L \times L}$ gathers all the corresponding channel gains on its main diagonal. Let $\mathbf{C} \triangleq \mathbf{P} \mathbf{V} \mathbf{A} = [\mathbf{c}_1, \mathbf{c}_2, \dots, \mathbf{c}_L] \in \mathbb{C}^{S \times L}$, eq. (27) can be rewritten as follows

$$\mathcal{C}_{\text{sum}}^{\text{NOMA}} = \log_2 \det \left(\mathbf{I}_S + \frac{1}{\sigma_w^2} \sum_{\ell=1}^L \mathbf{c}_\ell \mathbf{c}_\ell^H \right). \quad (28)$$

Since the diagonal matrices \mathbf{P} and \mathbf{A} are non-singular, we underline that $\text{rank}(\mathbf{C}) = \text{rank}(\mathbf{V})$.

On the other hand, the sum-rate capacity of the pure-OMA technique can be obtained from (26) by setting $G = L$, which implies $L_k = 1$, i.e., the L satellites with feasible links access the channel in an orthogonal manner, thus obtaining

$$\mathcal{C}_{\text{sum}}^{\text{OMA}} = \sum_{\ell=1}^L \rho_\ell \log_2 \det \left(\mathbf{I}_S + \frac{1}{\sigma_w^2 \rho_\ell} \mathbf{c}_\ell \mathbf{c}_\ell^H \right). \quad (29)$$

By virtue of the matrix determinant lemma [24], eq. (29) can be equivalently rewritten as

$$\begin{aligned} \mathcal{C}_{\text{sum}}^{\text{OMA}} &= \sum_{\ell=1}^L \rho_\ell \log_2 \left(1 + \frac{\|\mathbf{c}_\ell\|^2}{\sigma_w^2 \rho_\ell} \right) \\ &= \sum_{\ell=1}^L \rho_\ell \log_2 \left(1 + \mathcal{E}_p \frac{|A_\ell|^2}{\sigma_w^2 \rho_\ell} \right) \end{aligned} \quad (30)$$

where $\mathcal{E}_p \triangleq \sum_{s=0}^{S-1} p^2(s T_c)$. It is worth noticing that, in the pure-OMA case, the sum-rate capacity does not depend on the Doppler frequency shifts of the satellites.

Since the determinant is a log-concave function on the set of positive definite matrices, it follows from Jensen's inequality applied directly to (29) that $\mathcal{C}_{\text{sum}}^{\text{OMA}} \leq \mathcal{C}_{\text{sum}}^{\text{NOMA}}$, where we have also accounted for (7). The difference between $\mathcal{C}_{\text{sum}}^{\text{NOMA}}$ and $\mathcal{C}_{\text{sum}}^{\text{OMA}}$ is *exactly* zero if \mathbf{C} has rank one, that is, $\text{rank}(\mathbf{V}) = 1$, which happens when the L satellites with feasible ISLs towards the sink (see Definition 1) have exactly the same Doppler frequency shifts, i.e., $\bar{\nu} \triangleq \nu_1 = \nu_2 = \dots = \nu_L$. Indeed, in such a particular case, it results that $\mathbf{c}_\ell = A_\ell \mathbf{P} \bar{\mathbf{v}}$, $\forall \ell \in \{1, 2, \dots, L\}$, with $\bar{\mathbf{v}} \triangleq [1, e^{j2\pi\bar{\nu}}, \dots, e^{j2\pi\bar{\nu}(S-1)}]^T \in \mathbb{C}^S$, and, thus,

$$\mathcal{C}_{\text{sum}}^{\text{OMA}} = \mathcal{C}_{\text{sum}}^{\text{NOMA}} = \log_2 \left(1 + \frac{\mathcal{E}_p}{\sigma_w^2} \sum_{\ell=1}^L |A_\ell|^2 \right) \quad (31)$$

provided that the DoF fractions of the pure-OMA scheme in (29) are chosen as

$$\rho_\ell^{\text{OMA}} = \frac{|A_\ell|^2}{\sum_{q=1}^L |A_q|^2} \quad (32)$$

for $\ell \in \{1, 2, \dots, L\}$. As intuitively expected, in the case of equal Doppler frequency shifts, the largest sum-rate capacity is achieved with pure-OMA. However, the condition $\nu_1 = \nu_2 = \dots = \nu_L$

does not hold in practice since inter-OP ISLs exhibit significantly different Doppler frequency shifts (see Table I and the related discussion in Subsection III-D) and, in this context, pure-OMA is largely suboptimal in terms of sum-rate capacity.

B. Comparison between pure-NOMA and hybrid NOMA-OMA

A natural question arises about the advantage of performing a partition of the L satellites with feasible ISLs towards the sink in groups $\mathcal{L}_1, \mathcal{L}_2, \dots, \mathcal{L}_G$ over the pure-NOMA option. In this respect, let $\mathbf{C}_k \triangleq \mathbf{P} \mathbf{V}_k \mathbf{A}_k \in \mathbb{C}^{S \times L_k}$ and observe that $\mathbf{C}_1, \mathbf{C}_2, \dots, \mathbf{C}_G$ are matrices each gathering a different subset of the columns in \mathbf{C} , which will be referred to as *column matrices* of \mathbf{C} .

By using again the log-concavity of the determinant in the set of positive definite matrices, the following inequality comes from the application of the Jensen's inequality to (26):

$$\mathcal{C}_{\text{sum}} \leq \log_2 \det \left(\mathbf{I}_S + \frac{1}{\sigma_w^2} \sum_{k=1}^G \mathbf{C}_k \mathbf{C}_k^H \right) = \mathcal{C}_{\text{sum}}^{\text{NOMA}} \quad (33)$$

where we have used (7) and noticed that, since $\mathbf{C}_1, \mathbf{C}_2, \dots, \mathbf{C}_G$ are column matrices of \mathbf{C} , one has $\sum_{k=1}^G \mathbf{C}_k \mathbf{C}_k^H = \mathbf{C} \mathbf{C}^H$. Henceforth, the multiple access strategy where the L satellites are divided into groups of L_k satellites with NOMA within each group and OMA between the groups is suboptimal in terms of sum-rate capacity. Equality in (33) holds when the matrix $\mathbf{C}_k \mathbf{C}_k^H$ differs only for a scalar real constant, i.e., $\mathbf{C}_k \mathbf{C}_k^H = \chi_k \Omega$, $\forall k \in \{1, 2, \dots, G\}$, which in its turn would be fulfilled in the scenario where satellites belonging to the same group \mathcal{L}_k experience the same path losses, i.e., $|A_{\ell_{k,1}}|^2 = |A_{\ell_{k,2}}|^2 = \dots = |A_{\ell_{k,L_k}}|^2 = \chi_k$, $\forall k \in \{1, 2, \dots, G\}$, and, moreover, the groups $\mathcal{L}_1, \mathcal{L}_2, \dots, \mathcal{L}_G$ gather satellites with the same Doppler frequency shifts, i.e., $\mathbf{V}_k = \mathbf{V}'_k$, for each $k \neq k'$. In this case, one has $\mathcal{C}_{\text{sum}} = \mathcal{C}_{\text{sum}}^{\text{NOMA}}$, provided that the DoF fractions of the hybrid NOMA-OMA scheme in (26) are chosen as $\rho_k = \chi_k / \sum_{q=1}^G \chi_q$.

The performance gain of the pure-NOMA scheme over the hybrid NOMA-OMA one comes at the price of computation complexity, which in a pure-NOMA scheme grows with the number L of satellites having feasible ISLs with respect to the sink. Moreover, the available DoF are limited by the dimension S of the observable space [18] and, thus, there is no further DoF gain beyond having S satellites performing pure-NOMA concurrently. Interestingly, there is another aspect to be accounted for the specific scenario at hand. We have seen from Table I that some satellites with feasible ISLs towards the sink have the same Doppler frequency shift. Therefore, *what happens if there exist satellites with the same Doppler frequency shift that access the channel by using the pure-NOMA scheme?* According to (33), the pure-NOMA technique ensures the best possible sum-rate capacity even in this particular case. However, *what are the individual rates of*

the satellites with the same Doppler frequency shifts? To give an answer to this latter question, let us consider the two-satellite example, where the received signal (15) at the sink ends up to

$$\bar{\mathbf{r}}[u] = \tilde{\mathbf{h}}_1[u] b_1[u] + \tilde{\mathbf{h}}_2[u] b_2[u] + \mathbf{w}[u] \quad (34)$$

with $\tilde{\mathbf{h}}_\ell[u] \triangleq A_\ell e^{j2\pi S\nu_\ell u} \mathbf{P} \mathbf{v}_\ell \in \mathbb{C}^S$, for $\ell \in \{1, 2\}$ (the dependence on the group index k has been omitted since $G = 1$ in the pure-NOMA scheme). Assuming without loss of generality that satellite 1 is canceled first, the individual rates of the two satellites are given by $\mathcal{R}_\ell = \log_2(1 + \text{SINR}_\ell)$ (in bits/s/Hz), for $\ell \in \{1, 2\}$, where, starting from (18), after some algebraic manipulations, one has

$$\text{SINR}_1 \triangleq \frac{\sigma_w^2 |A_1|^2 \mathcal{E}_p + |A_1|^2 |A_2|^2 \left(\mathcal{E}_p^2 - |\mathbf{v}_1^H \mathbf{P}^2 \mathbf{v}_2|^2 \right)}{\sigma_w^2 (|A_2|^2 \mathcal{E}_p + \sigma_w^2)} \quad (35)$$

$$\text{SINR}_2 \triangleq |A_2|^2 \frac{\mathcal{E}_p}{\sigma_w^2} \quad (36)$$

with

$$|\mathbf{v}_1^H \mathbf{P}^2 \mathbf{v}_2|^2 = \left| \sum_{s=0}^{S-1} p^2(s T_c) e^{-j 2\pi s(\nu_1 - \nu_2)} \right|^2 \leq \mathcal{E}_p^2. \quad (37)$$

Equality in (37) holds when the two satellites have the same Doppler frequency shift, i.e., $\nu_1 = \nu_2$. Hence, we can infer that

$$\text{SINR}_1 \geq \text{SINR}_1^{\min} \triangleq \frac{|A_1|^2}{|A_2|^2 + \frac{\sigma_w^2}{\mathcal{E}_p}} \quad (38)$$

where SINR_1^{\min} is the SINR of satellite 1 in the case when the Doppler frequency shifts are equal. Two interesting conclusions can be drawn from (38). First, if the two satellites have different Doppler frequency shifts, i.e., $\nu_1 \neq \nu_2$, the satellite that is decoded first can benefit of a larger rate, compared to the case when $\nu_1 = \nu_2$. Second, in the high signal-to-noise ratio (SNR) regime, i.e., as $\mathcal{E}_p/\sigma_w^2 \rightarrow +\infty$, the rate of satellite 2 increases without bound, whereas the rate of satellite 1 tends approximately to 1 bit/s/Hz when, besides having the same Doppler frequency shift, the satellites experience comparable path losses, i.e., $|A_1| \approx |A_2|$.

In a nutshell, even though the pure-NOMA scheme exhibits the highest sum-rate capacity, it might result in a very unfair resource allocation, since basically the satellites having different Doppler frequency shifts might be allowed to achieve higher data rates with respect to those exhibiting equal Doppler frequency shifts. This suggests that, compared to the pure-NOMA scheme, the hybrid NOMA-OMA strategy may better capture fairness among satellites by judiciously partitioning them in groups on the basis of their Doppler frequency shifts, without appreciably degrading the sum-rate capacity. Next section studies such an insight in greater detail.

V. OPTIMIZATION OF THE HYBRID NOMA-OMA SCHEME

Along the same lines of Subsection III-D, we observe that $r_k \triangleq \text{rank}(\mathbf{C}_k) = \text{rank}(\mathbf{V}_k) \leq \min(S, L_k)$, where the equality holds if condition (22) is fulfilled, i.e., the Doppler frequency shifts of the satellites belonging to \mathcal{L}_k are distinct. Let $\mu_{k,1} \geq \mu_{k,2} \geq \dots \geq \mu_{k,r_k} > 0$ be the nonzero singular values of \mathbf{C}_k , eq. (26) can be written as

$$\mathcal{C}_{\text{sum}} = \sum_{k=1}^G \sum_{s=1}^{r_k} \rho_k \log_2 \left(1 + \frac{\mu_{k,s}^2}{\sigma_w^2 \rho_k} \right) \quad (39)$$

which shows that all the available per-group DoF can be exploited when r_k reaches its maximum value, given by $\min(S, L_k)$, i.e., the Doppler frequency shifts of the satellites belonging to \mathcal{L}_k are distinct, for each $k \in \{1, 2, \dots, G\}$. Consequently, we impose by design that the partition $\mathbb{P}(\mathcal{L})$ obeys $r_k = \min(S, L_k)$.

There are two design issues of the hybrid NOMA-OMA scheme to be faced with: (i) distribution of the available DoF among the satellites having feasible ISLs with respect to the sink, i.e., optimization of the variables $\rho_1, \rho_2, \dots, \rho_G$, subject to constraint (7); (ii) choice of the partition $\mathbb{P}(\mathcal{L})$, i.e., setting of G and definition of the satellite groups $\mathcal{L}_1, \mathcal{L}_2, \dots, \mathcal{L}_G$, subject to constraint $r_k = \min(S, L_k)$. Such optimization objectives are coupled to each other as shown soon after.

As a first step, by using the product rule of logarithms, we equivalently rewrite (39) as follows

$$\mathcal{C}_{\text{sum}} = \sum_{k=1}^G \rho_k \log_2 \left(\prod_{s=1}^{r_k} \left[1 + \frac{\mu_{k,s}^2}{\sigma_w^2 \rho_k} \right] \right) . \quad (40)$$

As a second step, by invoking the arithmetic-geometric mean inequality for non-negative real numbers [24], one obtains the following upper bound:

$$\mathcal{C}_{\text{sum}} \leq \sum_{k=1}^G r_k \rho_k \log_2 \left(1 + \frac{1}{\sigma_w^2 \rho_k} \left[\frac{1}{r_k} \sum_{s=1}^{r_k} \mu_{k,s}^2 \right] \right) \quad (41)$$

with equality if and only if the nonzero singular values of \mathbf{C}_k are all equal, i.e., the (spectral) condition number $\kappa(\mathbf{C}_k) \triangleq \mu_{k,1}/\mu_{k,r_k}$ is equal to 1 [24], for each $k \in \{1, 2, \dots, G\}$. The upper bound in (41) cannot be achieved in practice since $\kappa(\mathbf{C}_k) = 1$ if and only if $\mathbf{C}_k \mathbf{C}_k^H \propto \mathbf{I}_S$ and $S \leq L_k$ or $\mathbf{C}_k^H \mathbf{C}_k \propto \mathbf{I}_{L_k}$ and $S \geq L_k$. Henceforth, for the problem at hand, $\kappa(\mathbf{C}_k) > 1$ and, to maximize the sum-rate capacity, the design objective of the satellite groups is to ensure that $\mathbf{C}_1, \mathbf{C}_2, \dots, \mathbf{C}_G$ have condition numbers as close to 1 as possible. Moreover, recalling that the available DoF are limited by S , we design the partition $\mathbb{P}(\mathcal{L})$ such that each group has a number of satellites L_k smaller than or equal to S , i.e., we impose that $r_k = \min(S, L_k) = L_k$, for each $k \in \{1, 2, \dots, G\}$. To summarize, we came up with the following guideline for the design of the satellite groups $\mathcal{L}_1, \mathcal{L}_2, \dots, \mathcal{L}_G$.

Guideline D_g (Design of satellite groups): $\forall k \in \{1, 2, \dots, G\}$, form the group \mathcal{L}_k by selecting from the set \mathcal{L} , which gathers all the satellites with feasible ISLs towards the sink, L_k satellites such that:

- their Doppler frequency shifts are distinct, i.e., $r_k = \text{rank}(\mathbf{C}_k) = L_k$;
- $\kappa(\mathbf{C}_k)$ is close to 1 as possible.

The reformulation of the guideline D_g in terms of an algorithm with manageable complexity is pursued in Subsection V-A. For the time being, let us assume that D_g has been fulfilled such that we can regard the upper bound in (40) as a sharp approximation of the sum-rate capacity, i.e.,

$$\mathcal{C}_{\text{sum}} \approx \sum_{k=1}^G L_k \rho_k \log_2 \left(1 + \frac{1}{\sigma_w^2 L_k \rho_k} \sum_{s=1}^{L_k} \mu_{k,s}^2 \right). \quad (42)$$

Given the group sizes L_1, L_2, \dots, L_G , with $\sum_{k=1}^G L_k = L$, the problem of finding the values of the DoF fractions $\rho_1, \rho_2, \dots, \rho_G$, for which the approximation (42) of \mathcal{C}_{sum} is maximized, subject to (7), does not admit a closed-form solution. For such a reason, as a third step, we resort to a max-min approach. Specifically, we propose to maximize with respect to $\rho_1, \rho_2, \dots, \rho_G$, subject to (7), the lower bound

$$\mathcal{C}_{\text{sum}} \gtrapprox L_{\min} \sum_{k=1}^G \rho_k \log_2 \left(1 + \frac{1}{\sigma_w^2 L_k \rho_k} \sum_{s=1}^{L_k} \mu_{k,s}^2 \right). \quad (43)$$

with $L_{\min} \triangleq \min_{k \in \{1, 2, \dots, G\}} L_k$, where the approximation holds when the satellite groups have the same cardinality, i.e., L_k is independent of k . By Jensen's inequality [24], we know that

$$\sum_{k=1}^G \rho_k \log_2 \left(1 + \frac{1}{\sigma_w^2 L_k \rho_k} \sum_{s=1}^{L_k} \mu_{k,s}^2 \right) \leq \log_2 \left(1 + \frac{1}{\sigma_w^2} \sum_{k=1}^G \frac{1}{L_k} \sum_{s=1}^{L_k} \mu_{k,s}^2 \right) \quad (44)$$

where the upper bound is achieved when the DoF fractions are chosen as follows

$$\rho_k^{\text{hybrid}} = \frac{\frac{1}{L_k} \sum_{s=1}^{L_k} \mu_{k,s}^2}{\sum_{q=1}^G \frac{1}{L_q} \sum_{s=1}^{L_q} \mu_{q,s}^2} \quad (45)$$

for $k \in \{1, 2, \dots, G\}$, which represent the solution of the proposed max-min problem.

Having dealt with design issue (i), we provide in the forthcoming subsection a solution of issue (ii) according to D_g.

A. Choice of the satellite groups

Preliminarily, we observe that, since \mathbf{P} and \mathbf{A}_k are diagonal non-singular matrices, and \mathbf{V}_k is full rank under guideline D_g , one has

$$\begin{aligned} 1 < \kappa(\mathbf{C}_k) &\leq \kappa(\mathbf{P}) \kappa(\mathbf{V}_k) \kappa(\mathbf{A}_k) \\ &= \frac{p_{\max}}{p_{\min}} \frac{A_{k,\max}}{A_{k,\min}} \kappa(\mathbf{V}_k) \end{aligned} \quad (46)$$

with

$$p_{\min} \triangleq \min_{s \in \{0, 1, \dots, S-1\}} |p(s T_c)| \quad \text{and} \quad p_{\max} \triangleq \max_{s \in \{0, 1, \dots, S-1\}} |p(s T_c)| \quad (47)$$

$$A_{k,\min} \triangleq \min_{q \in \{1, 2, \dots, L_k\}} |A_{\ell_{k,q}}| \quad \text{and} \quad A_{k,\max} \triangleq \max_{q \in \{1, 2, \dots, L_k\}} |A_{\ell_{k,q}}|. \quad (48)$$

We note that p_{\min} and p_{\max} depend on the choice of the pulse-shaping filter $p(t)$ and sampling period T_c , and are not functions of k . For instance, in the case of rectangular pulse shaping, it follows that $p_{\min} = p_{\max} = 1$. On the other hand, $A_{k,\min}$ and $A_{k,\max}$ depend on the geometric path losses of the satellites belonging to the group \mathcal{L}_k , and they do not depend on the corresponding phase misalignments. The condition number of the Vandermonde matrix \mathbf{V}_k depends on the Doppler frequency shifts of the satellites belonging to \mathcal{L}_k .⁴ Since the singular values of a matrix are continuously depending on its entries, we expect that $\kappa(\mathbf{V}_k)$ grows if such Doppler frequency shifts become close to each other. To rigorously characterize such a behavior, a meaningful notion of distance between the Doppler frequency shifts is necessary. Since \mathbf{V}_k is a Vandermonde matrix on the unit circle, we can resort to the (normalized) arc length between points on the unit circle.

Definition 2 (*Wrap-around distance*). For $k \in \{1, 2, \dots, G\}$, let us define the *Doppler frequency shift set* $\mathcal{D}_k \triangleq \{\nu_{\ell_{k,1}}, \nu_{\ell_{k,2}}, \dots, \nu_{\ell_{k,L_k}}\}$ of the k -th satellite group \mathcal{L}_k . The wrap-around distance between two Doppler frequency shifts $\nu_{\ell_{k,q}}, \nu_{\ell_{k,q'}} \in \mathcal{D}_k$ is defined as follows

$$|\nu_{\ell_{k,q}} - \nu_{\ell_{k,q'}}|_{\mathcal{D}_k} \triangleq \min_{\eta \in \mathbb{Z}} |\nu_{\ell_{k,q}} - \nu_{\ell_{k,q'}} + \eta|. \quad (49)$$

The *minimal separation distance* δ_k of the Doppler frequency shift set \mathcal{D}_k is given by

$$\delta_k \triangleq \min_{\substack{\nu_{\ell_{k,q}}, \nu_{\ell_{k,q'}} \in \mathcal{D}_k \\ \nu_{\ell_{k,q}} \neq \nu_{\ell_{k,q'}}}} |\nu_{\ell_{k,q}} - \nu_{\ell_{k,q'}}|_{\mathcal{D}_k}. \quad (50)$$

It should be noted that, under assumption $f_{k,\max} T \ll 1$ (see Subsection II-C), it follows that $\delta_k \ll 1/S$, i.e., the Doppler frequency shifts in \mathcal{D}_k are *nearly colliding*. Inequality (46) and Definition 2 suggest the following reformulation of D_g .

⁴If the Doppler frequency shifts in \mathcal{L}_k lay on a fixed grid with width $1/S$ when $S \geq L_k$, then one would have a perfectly conditioned Vandermonde matrix, i.e., $\kappa(\mathbf{V}_k) = 1$.

Guideline D_g (Reformulation): $\forall k \in \{1, 2, \dots, G\}$, form the group \mathcal{L}_k by selecting from the set \mathcal{L} , which gathers all the satellites with feasible ISLs towards the sink, L_k satellites such that:

- their Doppler frequency shifts are distinct, i.e., $r_k = \text{rank}(\mathbf{C}_k) = L_k$;
- the minimal separation distance δ_k is maximized;
- their path losses are comparable, i.e., $A_{k,\max} \approx A_{k,\min}$.

On the basis of the discussion carried out in Subsection IV-B, the first two requirements (i.e., $\text{rank}(\mathbf{C}_k) = L_k$ and maximization of δ_k) avoid an unfair resource allocation within the group \mathcal{L}_k . Since the individual rates of the satellites also depend on their corresponding path losses, the third requirement $A_{k,\max} \approx A_{k,\min}$ goes on the direction of improving fairness among satellites belonging to the same group, too.

A strictly exhaustive procedure for finding the partition $\mathbb{P}(\mathcal{L})$ according to D_g is often computationally unmanageable, even for small values of L . In the subsequent two subsections, we propose two algorithms: in the former one, referred to as *Doppler-based partitioning*, we propose to partition the satellites into groups with the aim of creating high Doppler heterogeneity within each group and high Doppler similarity between groups (*anticlustering*), thus accounting for the first two requirements of D_g, without however considering the third requirement in terms of path losses; in the latter one, referred to as *max-fairness partitioning*, we propose to maximize a global fairness index, which implicitly accounts for all the three requirements of D_g, through an exhaustive search in suitably-reduced search space.

1) *Doppler-based partitioning:* Anticlustering consists of maximizing instead of minimizing a clustering objective function [25], [26]. For Doppler-based partitioning, we aim at maximizing the variance among Doppler features of the satellites with feasible ISLs towards the sink. In [27], it is shown that maximizing the variance directly minimizes the distances between the group centers. Therefore, we propose to determine the partition $\mathbb{P}(\mathcal{L})$ by maximizing the cost function:

$$\mathcal{V}(\mathcal{L}_1, \mathcal{L}_2, \dots, \mathcal{L}_G) \triangleq \sum_{k=1}^G \sum_{q=1}^{L_k} |f_{\ell_{k,q}} - \bar{f}_k|^2 \quad (51)$$

where $\bar{f}_k \triangleq \frac{1}{L_k} \sum_{q=1}^{L_k} f_{\ell_{k,q}}$ is the cluster center of the k -th group (so-called *k-means anticlustering*). Unfortunately, finding a partitioning that maximizes Doppler heterogeneity according to this criterion is still computationally challenging (i.e., it can be shown to be NP-hard). Indeed, the number of anticlustering partitions increases exponentially with L , quickly rendering it impossible

Algorithm 1: Doppler-based partitioning and subsequent DoF fraction assignment.

Input quantities: The set \mathcal{L} of the L satellites with feasible ISLs towards the sink within the considered observation interval and their corresponding Doppler frequency shifts f_1, f_2, \dots, f_L .

Output quantities: The partition $\mathbb{P}(\mathcal{L}) = \{\mathcal{L}_k\}_{k=1}^G$ of \mathcal{L} .

1. Set G equal to the number of satellites belonging to the same OP of the sink (they have equal Doppler frequency shifts very close to zero) and arbitrarily assign satellites to the G antoclusters by ensuring that each antocluster consists of (approximately) the same number of satellites.
2. Select the first satellite and check how (51) will change if the selected item is swapped with each satellite that is currently assigned to a different antocluster.
3. After performing each possible swap, realize the one that entails the most significant increase of (51). No swap is realized if the objective cannot be improved.
4. The procedure terminates when the swap operation has been repeated for each satellite.
5. Assign the DoF fractions to each group according to (45) (*optimized DoF assignment*) or set $\rho_k^{\text{hybrid}} = 1/G$ (*uniform DoF assignment*).

to find them all out in acceptable running time. For such a reason, we propose a low-complexity solution, which is based on a swap-based heuristic [28].

Our heuristic algorithm is based on swapping satellites between antoclusters such that each swap improves the objective function (51) by the largest possible margin. The proposed algorithm is summarized as Algorithm 1 at the top of next page. It can be shown [28] that Algorithm 1 performs very similarly to exact solution methods, e.g., integer linear programming, which ensure global optimal solution at the price of an exponential explosion of the running time even for small values of L . However, Algorithm 1 does not explicitly account for system fairness and the partition is determined without accounting for the available DoF.

2) *Max-fairness partitioning:* A simple yet informative index to quantify the fairness of a scheduling scheme was proposed in [29], which, according to (24), is given by

$$\mathcal{F}(\mathcal{L}_1, \mathcal{L}_2, \dots, \mathcal{L}_G) \triangleq \frac{\left[\sum_{k=1}^G \sum_{m=0}^{L_k-1} \rho_k \log_2 \left(1 + \text{SINR}_{k, \ell_{\max}^{(m)}}^{(m)} \right) \right]^2}{L \sum_{k=1}^G \sum_{m=0}^{L_k-1} \left[\rho_k \log_2 \left(1 + \text{SINR}_{k, \ell_{\max}^{(m)}}^{(m)} \right) \right]^2}. \quad (52)$$

Algorithm 2: Max-fairness joint partitioning and DoF fraction assignment.

Input quantities: The set \mathcal{L} of the L satellites with feasible ISLs towards the sink within the considered observation interval and their corresponding Doppler frequency shifts f_1, f_2, \dots, f_L .

Output quantities: The partition $\mathbb{P}(\mathcal{L}) = \{\mathcal{L}_k\}_{k=1}^G$ of \mathcal{L} .

1. Individuate the G satellites $\{\ell_{1,1}, \ell_{2,1}, \dots, \ell_{G,1}\} \subset \mathcal{L}$ that belong to the same OP of the sink (they have equal Doppler frequency shifts very close to zero) and perform the prepartitioning $\mathcal{L}_1 = \{\ell_{1,1}\}, \mathcal{L}_2 = \{\ell_{2,1}\}, \dots, \mathcal{L}_G = \{\ell_{G,1}\}$.
2. Generate a candidate solution by assigning the remaining $L - G$ satellites to the G group.
3. Assign the DoF fractions to each candidate group according to (45) (*optimized DoF assignment*) or set $\rho_k^{\text{hybrid}} = 1/G$ (*uniform DoF assignment*).
4. Evaluate the fairness index (52).
5. After performing Steps 2, 3, and 4 for all the possible partitions, choose the one that maximizes (52).

If all the L satellites get the same rate, then the fairness index is 1 and the multiple access method is said to be 100% fair. On the other hand, a multiple access scheme that favors only a few selected users has a fairness index tending to 0.

We propose to maximize (52) by resorting to a *reduced* exhaustive search. The possible partitions of the set \mathcal{L} is the Bell number $B_L = \frac{1}{e} \sum_{i=0}^{+\infty} \frac{i^L}{i!}$.⁵ For the example of Fig. 2, the size of the set \mathcal{L} is $L = 19$ and, in this case, there are $B_{19} = 5.832.742.205.057$ partitions to be generated and tested. To reduce the set of candidate partitions to a manageable size, the proposed procedure is based on a problem-specific preprocessing step that we call *prepartitioning*. In the prepartitioning step, we preliminarily identify the satellites that exhibit Doppler frequency shifts that are as similar as possible. According to Table I (see also Subsection III-D), they coincide with the satellites with feasible ISLs belonging to the same OP of the sink. Such satellites are assigned to different G groups and, thus, they operate according to the OMA scheme. So doing, the problem boils down to assign the remaining $L - G$ satellites to the G groups such that to maximize (52), whose number of possible partitions is given by G^{L-G} . In the case of Fig. 2 (see also Table I), one has $G = 8$ and, hence, there are $8^{19-8} = 8.589.934.592$ candidate partitions, which can be generated

⁵It can be interpreted as the L -th moment of a Poisson distribution with expected value 1.

and tested in a reasonable running time. The proposed algorithm is summarized as Algorithm 2 at the top of this page. It is noteworthy that Algorithm 2 jointly performs partitioning and DoF assignment to the satellite groups.

VI. NUMERICAL RESULTS

In this section, we provide numerical results aimed at corroborating the developed performance analysis and comparing the performance of the three multiple access schemes, namely, pure-OMA, pure-NOMA, and hybrid NOMA-OMA. To this aim, we consider the same simulation setting used to generate Fig. 2 and Table I (see Subsections II-A and III-D for details). We recall that, in this scenario, the number of satellites with feasible ISLs towards the sink is $L = 19$. The receiving device at the sink is affected by thermal noise with a noise figure of 7.9 dB. As performance metrics, we consider both the sum-rate capacity and the fairness index (52).

With reference to the pure-OMA scheme, we report the performance when DoF fractions are chosen according to (32), referred to as “pure-OMA (opt-DoF)”, as well as when they are allocated uniformly, i.e. $\rho_1 = \rho_2 = \dots = \rho_L = 1/L$, referred to as “pure-OMA (uni-DoF)”. In a similar way, we implement the two versions of the proposed hybrid NOMA-OMA technique optimized as in Algorithms 1 and 2 by assigning the DoF fractions in accordance with both (45), referred to as “hyb-NOMA-OMA-1 (opt-DoF)” and “hyb-NOMA-OMA-2 (opt-DoF)”, respectively, and the uniform rule $\rho_1 = \rho_2 = \dots = \rho_G = 1/G$, referred to as “hyb-NOMA-OMA-1 (uni-DoF)” and “hyb-NOMA-OMA-2 (uni-DoF)”, respectively.

First, we study the performance of the considered multiple access schemes when the oversampling factor at the sink is $S = 8$. Specifically, Table II reports the individual rates of all the satellites with feasible ISLs towards the sink, the sum-rate capacity, and the fairness index of the pure-NOMA and pure-OMA schemes. Besides significantly outperforming the pure-OMA technique in terms of sum-rate capacity (see Subsection IV-A), the pure-NOMA scheme also ensures a better fairness among the satellites when the pure-OMA DoF fractions are chosen as in (32). This is in accordance with [7]. If the pure-OMA DoF fractions are allocated uniformly, the sum-rate capacity of the pure-OMA scheme further cuts down but, however, it becomes almost 100% fair. Corroborating the analysis of Subsection IV-B, the results of Table II confirm the fact that, even though it is optimal in an information-theoretical sense, the pure-NOMA schemes is quite unfair when the transmissions of satellites with similar Doppler frequency shifts are superimposed.

In Table III, the individual rates of all the satellites with feasible ISLs towards the sink, the sum-rate capacity, and the fairness index of the hybrid NOMA-OMA scheme are shown. It is seen that Alg. 1 (opt-DoF), which performs a Doppler-based partitioning by using (45), substantially

TABLE II
INDIVIDUAL RATES OF THE $L = 19$ SATELLITES WITH FEASIBLE ISLS TOWARDS THE SINK, SUM-RATE CAPACITY, AND FAIRNESS INDEX OF PURE-NOMA AND PURE-OMA SCHEMES

Performance	pure-NOMA	pure-OMA (opt-DoF)	pure-OMA (uni-DoF)
\mathcal{R}_1	1.780	0.340	1.376
\mathcal{R}_2	1.617	0.956	1.454
\mathcal{R}_3	4.096	17.058	1.673
\mathcal{R}_4	2.112	3.443	1.551
\mathcal{R}_5	1.487	0.574	1.415
\mathcal{R}_6	1.570	0.227	1.345
\mathcal{R}_7	14.430	0.121	1.297
\mathcal{R}_8	17.806	0.089	1.274
\mathcal{R}_9	1.975	0.150	1.314
\mathcal{R}_{10}	2.214	0.308	1.368
\mathcal{R}_{11}	20.180	0.103	1.285
\mathcal{R}_{12}	0.914	0.183	1.329
\mathcal{R}_{13}	0.779	0.410	1.390
\mathcal{R}_{14}	0.623	1.640	1.495
\mathcal{R}_{15}	1.121	1.640	1.495
\mathcal{R}_{16}	0.503	0.410	1.390
\mathcal{R}_{17}	0.555	0.183	1.329
\mathcal{R}_{18}	0.999	0.103	1.285
\mathcal{R}_{19}	2.026	0.328	1.373
\mathcal{C}_{sum}	76.795	28.274	26.447
\mathcal{F}	0.316	0.135	0.994

ensures the same fairness index of the pure-NOMA scheme. However, when the hybrid NOMA-OMA scheme is designed by using Algorithm 1 with uniform DoF fractions, Alg. 1 (uni-DoF) is as fair as pure-OMA (uni-DoF), by remarkably assuring a sum-rate capacity increase of about 27 bits/s/Hz. Algorithm 2 allows the hybrid NOMA-OMA scheme to enhance network fairness at the price of a slight reduction of the sum-rate capacity compared to Alg. 1 (opt-DoF) and Alg. 1 (uni-DoF). For instance, Alg. 1 (opt-DoF) enhances the fairness index of 50% with respect to pure-NOMA scheme, while outperforming pure-OMA (opt-DoF) of about 30 bits/s/Hz, which represents the best trade-off between fairness and information rate for the methods under comparison.

Table IV gathers the partitions found by the different algorithms. It should be observed that, although the partition provided by Algorithm 1 does not depend on the DoF fractions, Alg. 1 (opt-DoF) and Alg. 1 (uni-DoF) return different partitions because the heuristic algorithm has been initialized differently for the two simulations. It can be inferred that the number of groups is $G = 8$, which is exactly the number of satellites with feasible ISLs belonging to the same OP of the sink (see Table I). Moreover, it is interesting to observe from a comparative analysis of

TABLE III

INDIVIDUAL RATES OF THE $L = 19$ SATELLITES WITH FEASIBLE ISLS TOWARDS THE SINK, SUM-RATE CAPACITY, AND FAIRNESS INDEX OF THE HYBRID NOMA-OMA SCHEME.

Performance	Alg. 1 (opt-DoF)	Alg. 2 (opt-DoF)	Alg. 1 (uni-DoF)	Alg. 2 (uni-DoF)
\mathcal{R}_1	0.831	2.213	2.835	2.835
\mathcal{R}_2	3.662	1.898	2.728	2.728
\mathcal{R}_3	15.206	2.804	3.254	2.980
\mathcal{R}_4	3.567	3.819	3.262	2.953
\mathcal{R}_5	14.959	3.753	2.940	2.940
\mathcal{R}_6	0.829	2.072	2.772	2.772
\mathcal{R}_7	0.278	7.634	2.926	2.926
\mathcal{R}_8	0.279	3.651	2.870	2.870
\mathcal{R}_9	0.726	3.482	2.965	2.965
\mathcal{R}_{10}	0.698	3.208	2.521	2.828
\mathcal{R}_{11}	2.065	3.744	2.897	2.897
\mathcal{R}_{12}	3.621	1.878	2.730	3.000
\mathcal{R}_{13}	0.789	1.444	3.146	2.876
\mathcal{R}_{14}	14.561	3.662	3.395	2.359
\mathcal{R}_{15}	0.355	3.246	0.414	3.125
\mathcal{R}_{16}	0.706	1.444	2.878	2.878
\mathcal{R}_{17}	0.021	0.643	3.000	3.000
\mathcal{R}_{18}	0.376	5.272	2.897	2.897
\mathcal{R}_{19}	0.894	2.292	2.871	3.106
\mathcal{C}_{sum}	64.432	58.167	53.310	54.945
\mathcal{F}	0.305	0.800	0.956	0.997

TABLE IV

PARTITION OF THE $L = 19$ SATELLITES WITH FEASIBLE ISLS TOWARDS THE SINK OF THE HYBRID NOMA-OMA SCHEME.

Scheme	Partition
Alg. 1 (opt-DoF)	$\mathcal{L}_1 = \{1, 19\}, \mathcal{L}_2 = \{2, 4, 12\}, \mathcal{L}_3 = \{3, 5, 14\}, \mathcal{L}_4 = \{6, 10, 13\}, \mathcal{L}_5 = \{7, 8\}, \mathcal{L}_6 = \{9, 16\}, \mathcal{L}_7 = \{11, 15\}, \mathcal{L}_8 = \{17, 18\}$
Alg. 2 (opt-DoF)	$\mathcal{L}_1 = \{4, 9, 11\}, \mathcal{L}_2 = \{2, 12\}, \mathcal{L}_3 = \{13\}, \mathcal{L}_4 = \{5, 14\}, \mathcal{L}_5 = \{10, 15\}, \mathcal{L}_6 = \{16\}, \mathcal{L}_7 = \{17\}, \mathcal{L}_8 = \{1, 3, 6, 7, 8, 18, 19\}$
Alg. 1 (uni-DoF)	$\mathcal{L}_1 = \{1, 11\}, \mathcal{L}_2 = \{2, 5, 13\}, \mathcal{L}_3 = \{3, 4, 14\}, \mathcal{L}_4 = \{6, 10, 18\}, \mathcal{L}_5 = \{7, 19\}, \mathcal{L}_6 = \{8, 12\}, \mathcal{L}_7 = \{9, 16\}, \mathcal{L}_8 = \{15, 17\}$
Alg. 2 (uni-DoF)	$\mathcal{L}_1 = \{6, 11\}, \mathcal{L}_2 = \{1, 12\}, \mathcal{L}_3 = \{7, 13\}, \mathcal{L}_4 = \{3, 14, 19\}, \mathcal{L}_5 = \{4, 8, 15\}, \mathcal{L}_6 = \{9, 16\}, \mathcal{L}_7 = \{10, 17\}, \mathcal{L}_8 = \{2, 5, 18\}$

Tables I and IV that even very small differences between the Doppler frequency shifts allow the satellites belonging to the same group to achieve non-negligible individual rates.

Finally, Figs. 3 and 4 depict the sum-rate capacity and the fairness index of the schemes under comparison as a function of the oversampling factor S at the sink. It can be argued that S has a large impact on the sum-rate capacity of the NOMA-based schemes, whereas the rate performance of the OMA-based techniques slightly improves for increasing values of S . In particular, the sum-rate capacity of hyb-NOMA-OMA-1 (opt-DoF) tends to diminish when the oversampling rate at

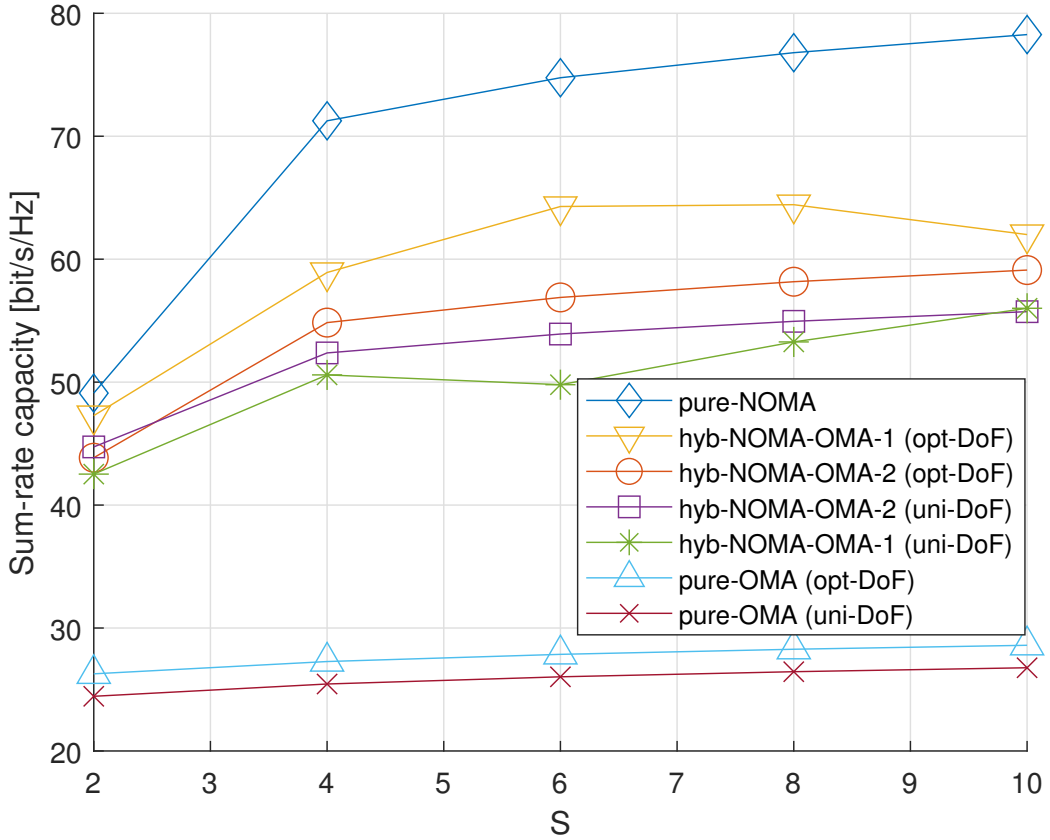


Fig. 3. Sum-rate capacity of the considered multiple access schemes as a function of S .

the sink becomes greater than the number $G = 8$ of the groups. On the other hand, the fairness index is slightly influenced by the values of S for all the considered schemes, especially for the pure-NOMA and pure-OMA techniques.

VII. CONCLUSIONS

In this paper, to ensure high spectral efficiency and massive connectivity in LEO constellations, we have studied the feasibility of superimposing the transmissions of satellites with different Doppler frequency profiles in a NOMA setting. To enhance network fairness, we have developed a theoretical framework that allows one to partition a pool of satellites into groups using orthogonal channel resources, with the goal of achieving high within-group heterogeneity in the Doppler frequency domain such that concurrent transmissions of satellites belonging to the same group can be separated at the sink through MMSE-SIC reception. Our numerical results show that the proposed hybrid NOMA-OMA scheme significantly outperforms existing OMA ones in terms of sum-rate capacity, by exhibiting a better trade-off between rate and fairness than the capacity-

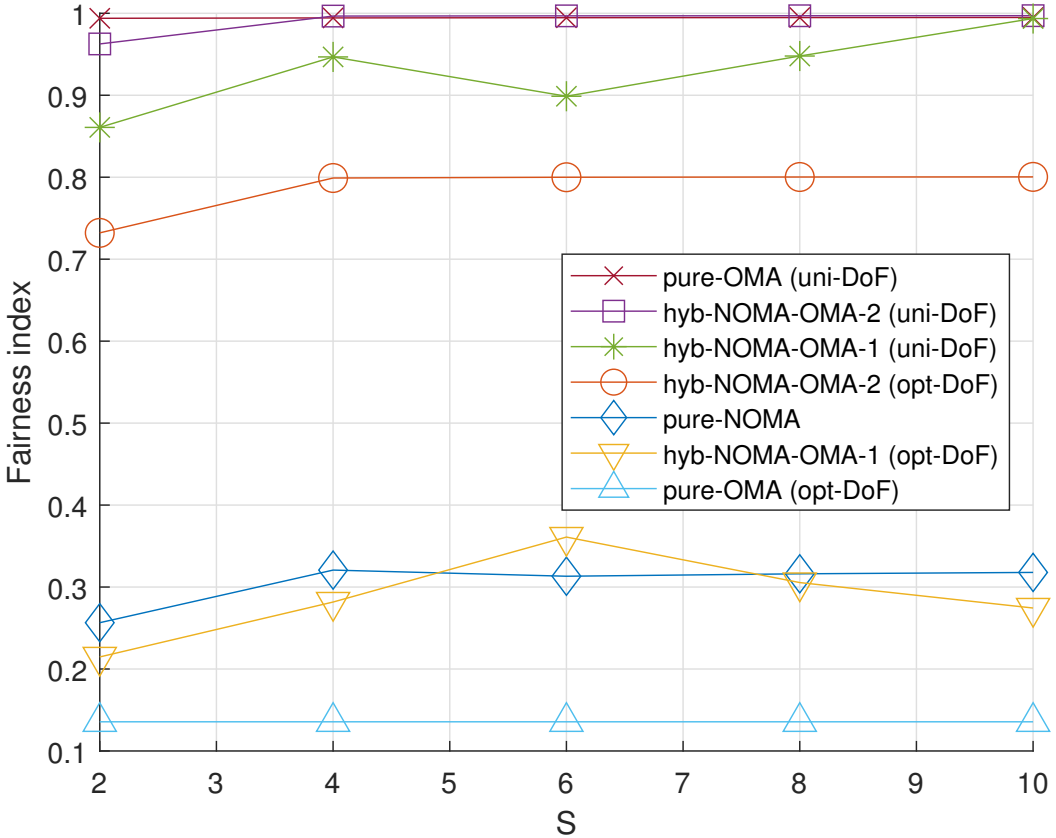


Fig. 4. Fairness index of the considered multiple access schemes as a function of S .

achieving pure-NOMA technique. Such a trade-off becomes significant in massive LEO systems, where a fair share of the scarce radio spectrum is one of the main concern.

REFERENCES

- [1] I. Leyva-Mayorga, B. Soret, M. Röper, D. Wübben, B. Matthiesen, A. Dekorsy, and P. Popovski, “LEO small-satellite constellations for 5G and beyond-5G communications,” *IEEE Access*, vol. 8, pp. 184 955–184 964, 2020.
- [2] T. Darwish, G. K. Kurt, H. Yanikomeroglu, M. Bellemare, and G. Lamontagne, “LEO satellites in 5G and beyond networks: A review from a standardization perspective,” *IEEE Access*, vol. 10, pp. 35 040–35 060, 2022.
- [3] J. Chu, X. Chen, C. Zhong, and Z. Zhang, “Robust design for NOMA-based multibeam LEO satellite internet of things,” *IEEE Internet of Things Journal*, vol. 8, no. 3, pp. 1959–1970, 2021.
- [4] A. U. Chaudhry and H. Yanikomeroglu, “Free Space Optics for Next-Generation Satellite Networks,” *IEEE Consumer Electronics Magazine*, vol. 10, no. 6, pp. 21–31, 2021.
- [5] I. Leyva-Mayorga, B. Soret, and P. Popovski, “Inter-plane inter-satellite connectivity in dense LEO constellations,” *IEEE Transactions on Wireless Communications*, vol. 20, pp. 3430–3443, 2021.
- [6] S. M. R. Islam, N. Avazov, O. A. Dobre, and K.-s. Kwak, “Power-domain non-orthogonal multiple access (NOMA) in 5G systems: Potentials and challenges,” *IEEE Communications Surveys & Tutorials*, vol. 19, no. 2, pp. 721–742, 2017.

- [7] W. Shin, M. Vaezi, B. Lee, D. J. Love, J. Lee, and H. V. Poor, “Non-orthogonal multiple access in multi-cell networks: Theory, performance, and practical challenges,” *IEEE Communications Magazine*, vol. 55, no. 10, pp. 176–183, 2017.
- [8] X. Yan, K. An, T. Liang, G. Zheng, Z. Ding, S. Chatzinotas, and Y. Liu, “The application of power-domain non-orthogonal multiple access in satellite communication networks,” *IEEE Access*, vol. 7, pp. 63 531–63 539, 2019.
- [9] Z. Gao, A. Liu, and X. Liang, “The performance analysis of downlink NOMA in LEO satellite communication system,” *IEEE Access*, vol. 8, pp. 93 723–93 732, 2020.
- [10] Z. Gao, A. Liu, C. Han, and X. Liang, “Sum rate maximization of massive MIMO NOMA in LEO satellite communication system,” *IEEE Wireless Communications Letters*, vol. 10, no. 8, pp. 1667–1671, 2021.
- [11] R. Ge, D. Bian, J. Cheng, K. An, J. Hu, and G. Li, “Joint user pairing and power allocation for NOMA-based GEO and LEO satellite network,” *IEEE Access*, vol. 9, pp. 93 255–93 266, 2021.
- [12] W. Tachikawa, K. Yoshii, and S. Shimamoto, “Performance analysis of uplink and downlink NOMA system in inter-satellite networks,” in *ICC 2021 - IEEE International Conference on Communications*, 2021, pp. 1–6.
- [13] Q. Hu, J. Jiao, Y. Wang, S. Wu, R. Lu, and Q. Zhang, “Multitype services coexistence in uplink NOMA for dual-layer LEO satellite constellation,” *IEEE Internet of Things Journal*, vol. 10, no. 3, pp. 2693–2707, 2023.
- [14] J. Pi, Y. Ran, H. Wang, Y. Zhao, R. Zhao, and J. Luo, “Dynamic planning of inter-plane inter-satellite links in LEO satellite networks,” in *ICC 2022 - IEEE International Conference on Communications*, 2022, pp. 3070–3075.
- [15] J. Liang, A. U. Chaudhry, and H. Yanikomeroglu, “Phasing parameter analysis for satellite collision avoidance in Starlink and Kuiper constellations,” in *2021 IEEE 4th 5G World Forum (5GWF)*, 2021, pp. 493–498.
- [16] J. G. Proakis, *Digital Communications*, 5th ed. McGraw Hill, 2007.
- [17] M. Civas and O. B. Akan, “Terahertz wireless communications in space,” 2021. [Online]. Available: <https://arxiv.org/abs/2110.00781>
- [18] D. Tse and P. Viswanath, *Fundamentals of Wireless Communication*. USA: Cambridge University Press, 2005.
- [19] A. Napolitano, *Generalizations of Cyclostationary Signal Processing: Spectral Analysis and Application*. John Wiley & Sons, Ltd. – IEEE Press, 2012.
- [20] D. Darsena, G. Gelli, I. Iudice, and F. Verde, “Detection and blind channel estimation for UAV-aided wireless sensor networks in smart cities under mobile jamming attack,” *IEEE Internet of Things Journal*, vol. 9, pp. 11 932–11 950, 2022.
- [21] 3GPP, “3rd Generation Partnership Project; Technical Specification Group Radio Access Network; Study on New Radio (NR) to Support Non Terrestrial Networks (Release 15),” 3rd Generation Partnership Project (3GPP), Technical Report (TR) 38.811, 09 2019, version 15.2.0.
- [22] P. Li, D. Paul, R. Narasimhan, and J. Cioffi, “On the distribution of SINR for the MMSE MIMO receiver and performance analysis,” *IEEE Transactions on Information Theory*, vol. 52, pp. 271–286, 2006.
- [23] B. D. and G. R., *Data Networks*. Englewood Cliffs: Prentice-Hall, 2001.
- [24] R. A. Horn and C. R. Johnson, *Matrix analysis*. Cambridge university press, 2012.
- [25] V. Valev, “Set partition principles,” in *Transactions of the ninth Prague conference on information theory, statistical decision functions, and random processes (Prague, 1982)*, 1983, pp. 251–256.
- [26] ——, “Set partition principles revisited,” in *Advances in Pattern Recognition: Joint IAPR International Workshops SSPR'98 and SPR'98 Sydney, Australia, August 11–13, 1998 Proceedings*. Springer, 1998, pp. 875–881.
- [27] H. Späth, “Anticlusetering: Maximizing the variance criterion,” *Control and Cybernetics*, vol. 15, no. 2, pp. 213–218, 1986.
- [28] M. Papenberg and G. W. Klau, “Using anticlusetering to partition data sets into equivalent parts.” *Psychological Methods*, vol. 26, no. 2, pp. 161–174, apr 2021.
- [29] R. Jain, D.-M. Chiu, and W. Hawe, “A quantitative measure of fairness and discrimination for resource allocation in shared computer systems,” *CoRR*, vol. cs.NI/9809099, 1998.